PUMA amplifies necroptosis signaling by activating cytosolic DNA sensors

Dongshi Chen[a,b], Jingshan Tong[a,b], Liheng Yang[a,b], Liang Wei[a,c], Donna B. Stolz[a,d], Jian Yu[a,c], Jianke Zhang[e], and Lin Zhang[a,b,1]

[a]UPMC Hillman Cancer Center, Pittsburgh, PA 15213; [b]Department of Pharmacology and Chemical Biology, University of Pittsburgh School of Medicine, Pittsburgh, PA 15213; [c]Department of Pathology, University of Pittsburgh School of Medicine, Pittsburgh, PA 15213; [d]Department of Cell Biology, University of Pittsburgh School of Medicine, Pittsburgh, PA 15213; and [e]Department of Microbiology and Immunology, Kimmel Cancer Center, Thomas Jefferson University, Philadelphia, PA 19107

Edited by Junying Yuan, Harvard Medical School, Boston, MA, and approved March 2, 2018 (received for review October 12, 2017)

Necroptosis, a form of regulated necrotic cell death, is governed by RIP1/RIP3-mediated activation of MLKL. However, the signaling process leading to necroptotic death remains to be elucidated. In this study, we found that *PUMA*, a proapoptotic BH3-only Bcl-2 family member, is transcriptionally activated in an RIP3/MLKL-dependent manner following induction of necroptosis. The induction of PUMA, which is mediated by autocrine TNF-α and enhanced NF-κB activity, contributes to necroptotic death in RIP3-expressing cells with caspases inhibited. On induction, PUMA promotes the cytosolic release of mitochondrial DNA and activation of the DNA sensors DAI/Zbp1 and STING, leading to enhanced RIP3 and MLKL phosphorylation in a positive feedback loop. Furthermore, deletion of *PUMA* partially rescues necroptosis-mediated developmental defects in *FADD*-deficient embryos. Collectively, our results reveal a signal amplification mechanism mediated by PUMA and cytosolic DNA sensors that is involved in TNF-driven necroptotic death in vitro and in vivo.

PUMA | necroptosis | RIP3 | MLKL | NF-κB

Necroptosis has recently emerged as a critical regulated form of necrotic cell death in physiology and human diseases (1–4). Necroptosis can be triggered by various extracellular stimuli known to activate inflammation and cell death. Distinctive from apoptosis, necroptosis is morphologically characterized by early loss of plasma membrane integrity, leakage of intracellular contents, and organelle swelling (1). Induction of necroptosis is controlled by two essential serine-threonine kinases, RIP1 and RIP3 (5, 6). On induction of necroptosis, RIP1 and RIP3 form a functional amyloid signaling complex (7) that recruits mixed-lineage kinase domain-like protein (MLKL) to initiate the process of cell death (8). Although RIP1/RIP3-mediated signaling has been extensively studied, the effectors and molecular events in the signal amplification and execution of necroptosis remain unclear (9).

Bcl-2 family proteins are evolutionarily conserved cell death regulators that include prosurvival members, such as Bcl-2 and Bcl-X_L, and the proapoptotic members Bax/Bak and BH3-only proteins (10). In apoptosis, these proteins control mitochondrial outer membrane permeabilization (MOMP), which leads to caspase activation and execution of cell death. PUMA is a BH3-only Bcl-2 family protein that mediates the apoptotic response to a variety of stress conditions, including DNA damage, oncogene activation, inflammation, and viral infection (11). In response to these conditions, *PUMA* is transcriptionally activated by p53, Forkhead Box O3a (FOXO3a), p73, c-Myc, E2F1, or NF-κB (11). It binds to prosurvival Bcl-2 proteins to activate Bax and Bak and promote MOMP and caspase activation. Several studies have suggested that Bcl-2 family proteins are also involved in regulating necroptosis (12, 13); however, their role in non-apoptotic death is not well understood.

Our previous studies showed that PUMA can be induced by NF-κB in response to inflammation and TNF-α (14, 15), which can trigger necroptosis in cells in which caspases are inhibited (5). Thus, we investigated a potential role of PUMA in necroptosis. Our results demonstrate that PUMA is activated in a RIP3/MLKL-dependent manner and promotes signal amplification in TNF-driven necroptosis in vitro and in vivo in a positive feedback loop.

Results

***PUMA* Is Transcriptionally Activated During RIP1/RIP3-Dependent Necroptosis.** RIP1/RIP3-dependent necroptosis can be induced in HT29 colon cancer cells in response to inhibitor of apoptosis protein (IAP) inhibition by SMAC mimetics and caspase inhibition by caspase inhibitors (5). We treated HT29 cells with the SMAC mimetic LBW-242 (L) and the pan-caspase inhibitor z-VAD-fmk (z-VAD; Z) to induce necroptosis. Induction of necroptosis was analyzed by several methods (Fig. 1*A*), including loss of cell viability by crystal violet staining (5), depletion of intracellular ATP (5), propidium iodide (PI) staining for non-apoptotic death, extracellular release of nuclear High-Mobility Group Box 1 (HMGB1) (16), and inhibition of cell death by the RIP1 inhibitor necrostatin-1 (Nec-1; N) (17). Analysis of Bcl-2 family proteins revealed a marked induction of PUMA in HT29 cells after treatment with L+Z, but not after treatment with either compound alone (Fig. 1*A*). Both PUMA protein and mRNA were induced in a time-dependent fashion following L+Z treatment (Fig. 1*B*). In addition to PUMA, Bcl-X_L was also

Significance

Necroptosis is a regulated form of necrotic cell death that is important in physiology and human diseases. However, the signaling process leading to eventual cell death in necroptosis remains unclear. We show that *PUMA*, a proapoptotic BH3-only Bcl-2 family member, is induced and plays a role in necroptotic death. PUMA induction enhances necroptotic signaling by promoting the release of mitochondrial DNA and activation of cytosolic DNA sensors. We provide genetic evidence for the functional role of PUMA in necroptosis-mediated developmental defects in mice. Our results demonstrate a previously unknown function of Bcl-2 family proteins and reveal a signal amplification mechanism mediated by PUMA and cytosolic DNA sensors that is involved in TNF-driven necroptosis in vitro and in vivo.

Author contributions: D.C., J.Y., and L.Z. designed research; D.C., J.T., L.Y., and L.W. performed research; D.C., J.T., L.Y., L.W., D.B.S., J.Y., J.Z., and L.Z. contributed new reagents/analytic tools; D.C., D.B.S., J.Y., J.Z., and L.Z. analyzed data; and D.C. and L.Z. wrote the paper.

The authors declare no conflict of interest.

This article is a PNAS Direct Submission.

[1]To whom correspondence should be addressed. Email: zhanglx@upmc.edu.

This article contains supporting information online at www.pnas.org/lookup/suppl/doi:10.1073/pnas.1717190115/-/DCSupplemental.

Published online March 26, 2018.

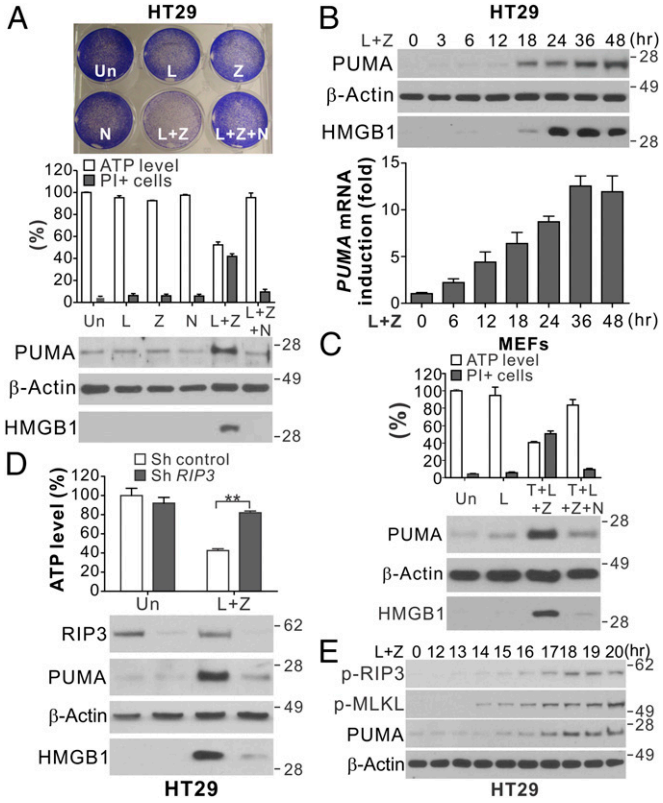

Fig. 1. PUMA is induced in RIP1/RIP3-dependent necroptosis. (*A*) HT29 colon cancer cells were treated with the control DMSO (Un), LBW242 (L; 2 μM), z-VAD (Z; 10 μM), Necrostatin-1 (N; 20 μM), or the indicated combinations. (*Upper*) Crystal violet staining at 48 h. (*Middle*) ATP levels and PI staining at 48 h. (*Lower*) Western blots of PUMA in cell lysates and HMGB1 in 20 μL of cell culture medium at 24 h. (*B*) HT29 cells were treated with LBW242 and z-VAD (L+Z) as in *A*. (*Upper*) PUMA expression and HMGB1 release. (*Lower*) *PUMA* mRNA expression. (*C*) MEFs were treated with LBW242 (L; 2 μM), alone or in combination with TNF-α (T; 20 ng/mL), z-VAD (Z; 10 μM), or Necrostatin-1 (N; 20 μM). ATP levels and PI staining (*Upper*) and PUMA expression and HMGB1 release (*Lower*) were analyzed as in *A*. (*D*) HT29 cells stably expressing control or *RIP3* shRNA were treated and analyzed as in *A*. (*E*) Western blots of phospho-RIP3 (p-RIP3; S227), phospho-MLKL (p-MLKL; S358), and PUMA in HT29 cells treated with L+Z at the indicated time points. Values in *A*–*D* are expressed as mean ± SD. $n = 3$. $^{**}P < 0.01$.

induced, while other Bcl-2 family members, including Bcl-2, Mcl-1, Bax, Bid, Bim, and Bad, were not significantly changed (Fig. S1 *A* and *B*). PUMA induction was detected in mouse embryonic fibroblast (MEF) cells undergoing necroptosis induced by TNF-α, LBW-242, and z-VAD (T+L+Z) (Fig. 1*C*) (18). The time course and extent of PUMA induction were found to correlate with HMGB1 release in both HT29 cells and MEFs (Fig. 1*B* and Fig. S1*C*).

The treatment with RIP1 inhibitor Nec-1 abolished PUMA induction in both HT29 cells and MEFs undergoing necroptosis, coinciding with restoration of cell viability and suppression of HMGB1 release (Fig. 1 *A* and *C*). Knockdown of *RIP1* or *RIP3* by shRNA suppressed induction of PUMA and necroptosis by L+Z in HT29 cells (Fig. 1*D* and Fig. S1*D*). PUMA induction was detectable at 1–2 h after RIP3 S227 phosphorylation (Fig. 1*E*), an early event in necroptosis signaling (4). While RIP1 is ubiquitously expressed, RIP3 is often epigenetically silenced in cancer cell lines (19), and its expression determines whether cells can undergo necroptosis (5). Our analysis of 16 cell lines identified several colon cancer cell lines that express RIP3 in addition to HT29 (Fig. S1*E*). Induction of PUMA and necroptosis was observed in RIP3-expressing LoVo and SW1463 cells following L+Z treatment and blunted by Nec-1 (Fig. S1*F*), but not in HCT116 and RKO cells lacking RIP3 (Fig. S1*G*). RIP1-dependent induction of PUMA and Bcl-X_L was also found in necroptosis induced by TNF-α and LBW-242 (T+L) in *FADD* null Jurkat cells (Fig. S1*H*). These results indicate that *PUMA* is transcriptionally activated during RIP1/RIP3-dependent necroptosis in different cell types.

PUMA Induction Requires MLKL and Is Mediated by Autocrine TNF-α and Enhanced NF-κB Activity. We investigated the mechanism of PUMA induction during necroptosis. Execution of necroptosis is characterized by formation of the necrosome complex and activation of MLKL through its phosphorylation (8). PUMA induction by L+Z in HT29 cells was detectable shortly after the onset of RIP3-dependent MLKL phosphorylation (Fig. 1*E* and Fig. S1*I*) and was suppressed by *MLKL* knockdown (Fig. 2*A* and Fig. S1*J*) or the MLKL inhibitor necrosulfonamide (NSA; Fig. 2*B*) (8). PUMA induction in necroptosis is unrelated to p53, STAT1, p73, FOXO3a, or E2F1 (Fig. S2 *A*–*C*). We previously showed that PUMA can be induced by the p65 subunit of NF-κB in response to TNF-α (15). Knockdown of *p65* suppressed PUMA induction and necroptosis in HT29 and SW1463 cells treated with L+Z (Fig. 2*C* and Fig. S2*D*). *p65* knockout (KO) in MEFs also abrogated PUMA induction, but did not inhibit cell death induced by T+L+Z (Fig. S2*E*). Treating HT29 cells with L+Z induced p65 nuclear translocation (Fig. S2*F*), p65 binding to the *PUMA* promoter (Fig. 2*D*), and activation of a *PUMA* promoter reporter via an NF-κB binding site (Fig. S2*G*) (15).

It has been shown that NF-κB can be activated by RIP1 in necroptosis signaling (20). We detected two phases of NF-κB activation by p65 phosphorylation (S536) (Fig. 2*E*). The first phase occurred at 3–12 h and was *RIP1*-dependent (Fig. S2*H*), but it did not correlate with MLKL phosphorylation or PUMA induction after 12 h (Fig. 2*E*) and was not affected by MLKL knockdown or inhibition (Fig. 2 *A* and *B*). The second phase of p65 phosphorylation after 12 h was MLKL-dependent (Fig. 2 *A* and *B*) and consistent with MLKL phosphorylation and PUMA induction (Fig. 2*E*). The enhanced NF-κB activity and PUMA induction were due to autocrine TNF-α, as *TNF-α* mRNA and secretion were markedly increased at 12–18 h and were suppressed by MLKL knockdown or inhibition (Fig. 2*F* and Fig. S2*I*). Extracellular addition of the anti-TNF antibody infliximab (Remicade) abolished the enhanced p65 phosphorylation and PUMA induction, as well as necroptosis, in HT29 cells treated with L+Z (Fig. S2*J*). Furthermore, activation of the *PUMA* promoter by L+Z could be suppressed by inhibition of TNF, RIP1, MLKL, or NF-κB (Fig. S2*G*). These results indicate that *PUMA* is directly activated by NF-κB via autocrine TNF-α at the early execution stage of necroptosis following MLKL activation.

PUMA Contributes to Necroptosis in RIP3-Expressing Cells with Caspase Inhibition. We asked whether PUMA plays a functional role in necroptotic death. Knockdown of *PUMA* by shRNA or siRNA largely suppressed cell viability loss, ATP depletion, PI staining, and HMGB1 release in HT29, LoVo, and SW1463 cells treated with necroptotic stimuli (Fig. 3*A* and Fig. S3*A*). HT29 cells with *PUMA* KO by CRISPR/Cas9 showed similar phenotypes as *PUMA*-knockdown cells (Fig. S3*B*). TEM analysis showed *PUMA*-knockdown cells lacked morphological signs of necroptosis observed in the control cells, including plasma membrane permeabilization, translucent cytosol, and swollen mitochondria (1) (Fig. 3*B*). Interestingly, PUMA depletion suppressed the enhanced RIP3 and MLKL phosphorylation after onset at 12–14 h following L+Z treatment (Fig. 3 *A* and *C*), suggesting that PUMA induction provides positive feedback to RIP3 and MLKL to amplify the necroptosis signal.

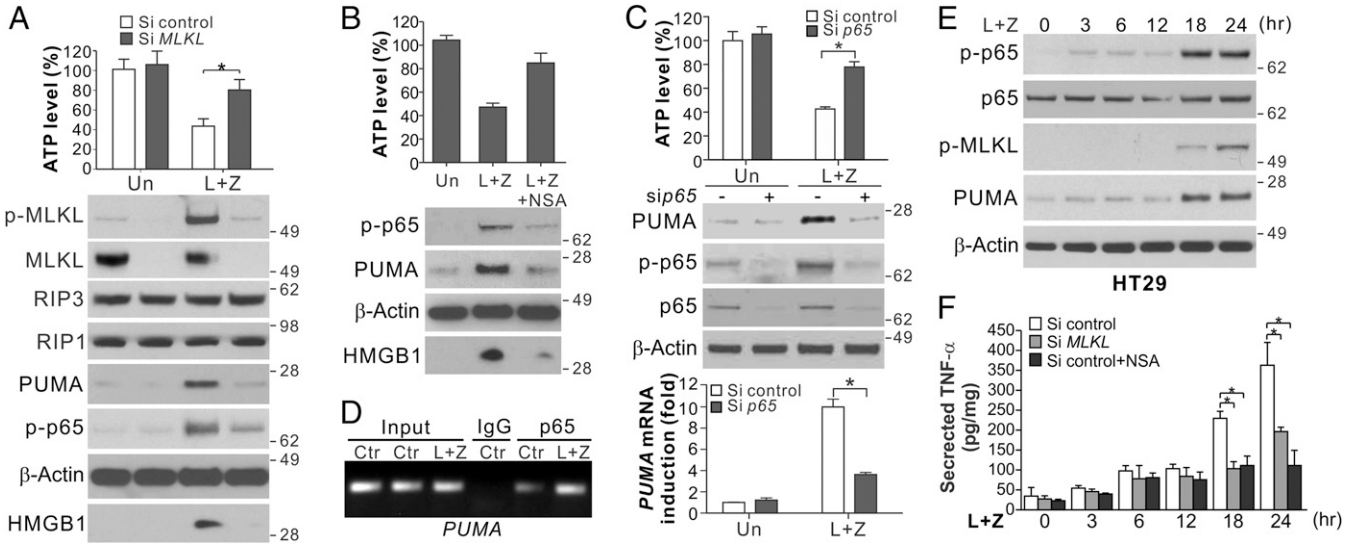

Fig. 2. Induction of PUMA is mediated by NF-κB downstream of MLKL. (*A*) HT29 cells transfected with control scrambled or *MLKL* siRNA were treated with L+Z. (*Upper*) ATP levels at 48 h. (*Lower*) Protein expression and HMGB1 release at 24 h. (*B*) HT29 cells with or without pretreatment with NSA (1 μM) were treated and analyzed as in *A*. (*C*) HT29 cells transfected with control scrambled or *p65* siRNA were treated with L+Z as in *A*. ATP levels at 24 h (*Upper*), indicated proteins at 48 h (*Middle*), and *PUMA* mRNA expression at 24 h (*Lower*) were analyzed. (*D*) Chromatin immunoprecipitation (ChIP) analysis of the binding of p65 to the *PUMA* promoter in HT29 cells treated as in *A* for 24 h. (*E*) Western blots of total and phospho-p65 (p-p65; S536) at indicated time points in HT29 cells treated as in *A*. (*F*) *TNF-α* secretion at indicated time points in HT29 cells treated as in *A*. Values in *A–C* and *F* are expressed as mean ± SD. $n = 3$. $^*P < 0.05$.

The pan-kinase inhibitor staurosporine (STS), a widely used apoptosis inducer, can induce necroptosis under certain conditions (21). PUMA can be induced by STS and contributes to STS-induced apoptosis (22). *PUMA* depletion suppressed STS-induced and RIP3/MLKL-dependent necroptosis in RIP3-expressing HT29 and LoVo cells with caspase inhibition (Fig. S3 *C–F*), but not in HCT116 cells lacking RIP3 (Fig. S3*G*). PUMA induction also contributed to the necroptosis induced by T+L in *FADD* null Jurkat cells (Fig. S3*H*). *PUMA* KO in MEFs suppressed the necroptosis induced by T+L+Z (Fig. 3*D*) or enforced RIP3 dimerization (23) (Fig. S4 *A* and *B*). Furthermore, *PUMA* KO modestly reduced the necroptosis induced by relatively high doses of TNF-α and z-VAD (T+Z) (24), but had little or no effect on that induced by bacterial lipopolysaccharides (LPS) or Poly I:C in MEFs and bone marrow-derived macrophages (BMDMs) (Fig. S4 *C* and *D*), which could be blocked by *RIP3* or *MLKL* KO (24).

We then tested whether PUMA induction alone is sufficient to induce necroptosis. Infection of HT29 and HCT116 cells with PUMA-expressing adenovirus (Ad-PUMA), but not with adenovirus expressing BH3-deleted PUMA, induced apoptosis detected by nuclear fragmentation and caspase activation (Fig. 4 *A* and *B* and Fig. S5). Caspase inhibition by z-VAD in conjunction with Ad-PUMA infection changed the mode of death in HT29 cells from apoptosis to necroptosis, as demonstrated by blockage of nuclear fragmentation and caspase 3 cleavage but increases in HMGB1 release, PI staining, and RIP3 and MLKL phosphorylation (Fig. 4*A*). Plasma membrane permeabilization, translucent cytosol, and swollen mitochondria were detected in HT29 cells undergoing necroptosis induced by Ad-PUMA + z-VAD (Fig. 4*B*). Knockdown of RIP3 or MLKL suppressed the necroptotic death induced by Ad-PUMA + z-VAD (Fig. 4 *C* and *D*). In contrast, z-VAD treatment completely blocked the PUMA-induced death of HCT116 cells, without HMGB1 release or morphological signs of necroptosis (Fig. S5). These results demonstrate that PUMA by itself can promote RIP3/MLKL-dependent necroptosis in RIP3-expressing cells with caspase inhibition.

PUMA Provides Positive Feedback to RIP3/MLKL by Promoting Cytosolic Release of Mitochondrial DNA and Activation of DNA Sensors. The requirement for its BH3 domain (Fig. 4*A*) suggests that PUMA mediates necroptosis through its interactions with other Bcl-2

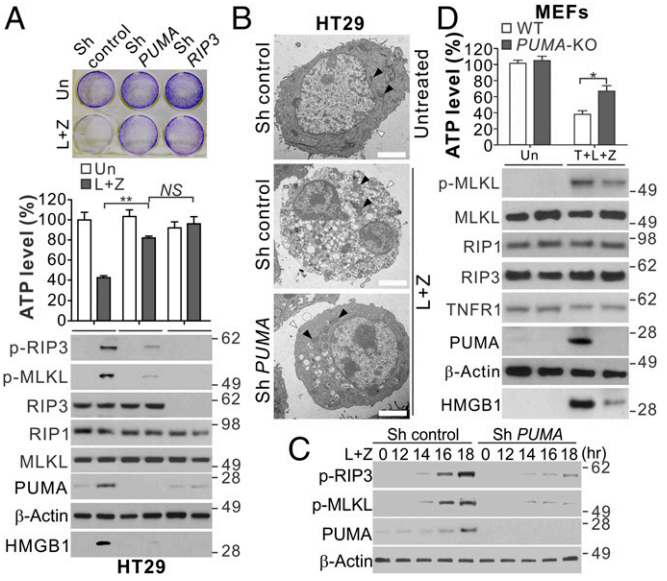

Fig. 3. PUMA induction contributes to necroptosis and enhanced RIP3 and MLKL phosphorylation in RIP3-expressing cells with caspase inhibition. (*A*) HT29 cells expressing control, *PUMA*, or *RIP3* shRNA were treated with L+Z. (*Upper*) Crystal violet staining at 48 h. (*Middle*) ATP levels at 48 h. (*Lower*) Western blots of indicated proteins and HMGB1 release at 24 h. (*B*) Representative TEM pictures of HT29 cells treated as in *A* for 24 h. Black arrowheads indicate mitochondria, and white arrowheads indicate plasma membranes. (Scale bars: 2 μm.) (*C*) Western blots of indicated proteins in HT29 cells transfected with control or *PUMA* shRNA treated with L+Z. (*D*) WT and *PUMA* KO MEFs were treated with 20 ng/mL TNF-α, 2 μM LBW242, and 10 μM z-VAD (T+L+Z) and analyzed as in *A*. Values in *A* and *D* are expressed as mean ± SD. $n = 3$. *NS*, $P > 0.05$; $^*P < 0.05$; $^{**}P < 0.01$.

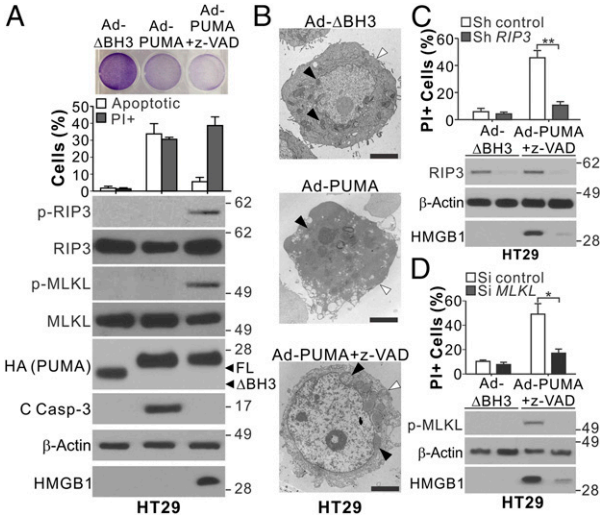

Fig. 4. PUMA expression alone can induce necroptosis and RIP3 and MLKL phosphorylation in RIP3-expressing cells with caspase inhibition. (*A*) HT29 cells with or without pretreatment with 10 μM z-VAD were infected with control (BH3 domain deleted; ΔBH3) or PUMA-expressing adenovirus (Ad-PUMA). (*Upper*) Crystal violet staining at 24 h. (*Middle*) analysis of apoptosis and PI staining at 48 h. (*Lower*) Western blots of indicated proteins and HMGB1 release at 24 h. (*B*) Representative TEM pictures of HT29 cells treated as in *A* for 24 h. Black arrowheads indicate mitochondria, and white arrowheads indicate plasma membranes. (Scale bars: 2 μm.) (*C*) HT29 cells stably transfected with control or *RIP3* shRNA were treated and analyzed as in *A*. (*D*) HT29 cells transfected with control scrambled or *MLKL* siRNA were treated and analyzed as in *A*. Values in *A*, *C*, and *D* are expressed as mean ± SD. $n = 3$. $^*P < 0.05$; $^{**}P < 0.01$.

family proteins, such as Bcl-X_L, which was induced by L+Z (Fig. S1 *A*, *B*, and *H*). Bcl-X_L transfection suppressed necroptosis in HT29 cells (Fig. S6*A*), whereas its knockdown enhanced necroptosis and abrogated the effect of PUMA knockdown (Fig. S6 *B* and *C*), suggesting that PUMA promotes necroptosis by antagonizing Bcl-X_L. However, knockdown of *BAX* and *BAK* in HT29 cells did not affect necroptosis and RIP3/MLKL phosphorylation induced by Ad-PUMA + z-VAD (Fig. S6*D*). *BAX*/*BAK* double-KO (DKO) MEFs had intact necroptosis, PUMA induction, and MLKL phosphorylation in response to T+L+Z (Fig. S6*E*); therefore, Bax/Bak-mediated MOMP, a key feature of apoptosis, is not involved in PUMA-mediated necroptosis.

Interestingly, we detected cytosolic release of mitochondrial DNA in both HT29 cells and MEFs undergoing necroptosis, as indicated by enhanced cytosolic DNA staining (green), as well as reduced colocalization (yellow) of mitochondria (red) and DNA, which is correlated with reduced mitochondrial interconnectivity and elongation (Fig. 5*A* and Fig. S6*F*). Genomic PCR analysis confirmed the release of mitochondrial *cytochrome B* (*CytB*) DNA into the cytosol of necroptotic HT29 cells and MEFs (Fig. 5*B* and Fig. S6*G*). The release of mitochondrial DNA was dependent on PUMA and was suppressed in PUMA-depleted HT29 and *PUMA* KO MEFs (Fig. 5 *A* and *B* and Fig. S6 *F* and *G*). Depleting mitochondrial DNA by ethidium bromide (EB) treatment suppressed the necroptosis induced by L+Z in HT29 cells (Fig. S7 *A* and *B*).

Exogenous viral DNA and endogenous self-DNA in the cytosol can trigger activation of DNA sensors, such as DAI/Zbp1 and cGAS/STING (25), which are involved in necroptosis (26, 27). Our analysis of several DNA sensors detected induction of *DAI*/*Zbp1* mRNA and protein in HT29 cells and MEFs undergoing necroptosis, as well as depletion of STING (Fig. 5*C* and Fig. S7*C*), which is known to be rapidly degraded following cGAS-mediated activation in response to cytosolic DNA (28). These changes in DNA sensors were abrogated in PUMA-deficient HT29 cells and MEFs (Fig. 5*C* and Fig. S7 *D* and *E*). Treatment of HT29 cells with Ad-PUMA + z-VAD also induced DAI/Zbp1 expression and STING degradation (Fig. 5*D*). Enhanced binding of DAI/Zbp1 to

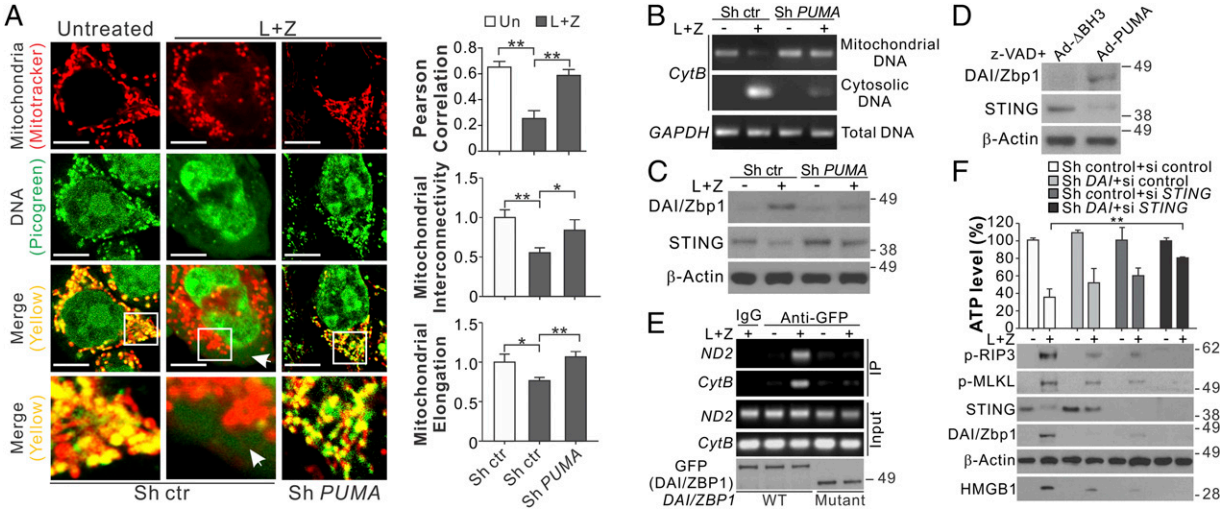

Fig. 5. PUMA promotes mitochondrial DNA release and activates DNA sensors to enhance RIP3/MLKL activation in necroptosis. (*A*) HT29 cells stably expressing control or *PUMA* shRNA were treated with L+Z for 24 h. Cells were analyzed by confocal microscopy after mitochondria staining with MitoTracker (red) and DNA staining with PicoGreen (green). (*Left*) Representative pictures with the arrow indicating cytoplasmic DNA. (Scale bars: 5 μm.) (*Right*) Quantification of colocalization of MitoTracker and PicoGreen staining and mitochondrial interconnectivity and elongation by Image J software in at least 20 randomly selected individual cells. (*B*) Mitochondrial and cytosolic fractions isolated from an equal number of HT29 cells treated as in *A* were analyzed by genomic PCR for *CytB*. (*C*) Western blots of DAI/Zbp1 and STING in HT29 cells treated as in *A*. (*D*) Western blots of DAI/Zbp1 and STING in HT29 cells infected with control (Ad-ΔBH3) or PUMA-expressing adenovirus (Ad-PUMA) and treated with 10 μM z-VAD for 24 h. (*E*) HT29 cells transfected with GFP-tagged full-length DAI/Zbp1 (WT) or a deletion mutant of its N-terminal DNA binding domain (mutant) were treated with L+Z as in *A*. Transfected DAI/Zbp1 was examined by Western blot analysis (*Lower*) and pulled down by IP with anti-GFP antibody, followed by PCR analysis of mitochondrial *CytB* and *ND2* DNA. (*F*) HT29 cells stably expressing control or *DAI*/*Zbp1* shRNA were transfected with control scrambled or *STING* siRNA and then treated as in *A*. (*Upper*) ATP levels at 48 h. (*Lower*) Western blots of indicated proteins and HMGB1 release at 24 h. Values in *F* are expressed as mean ± SD. $n = 3$. $^*P < 0.05$; $^{**}P < 0.01$.

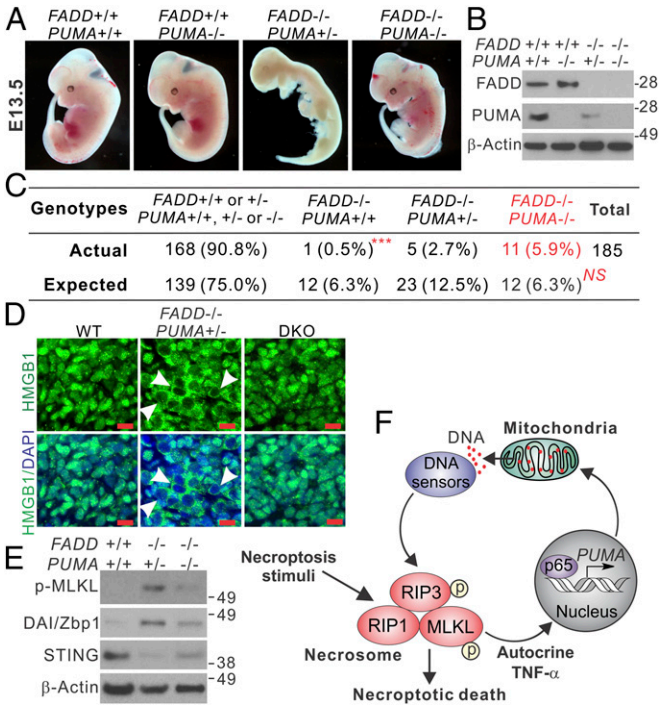

Fig. 6. PUMA deficiency rescues defective embryonic development and suppresses necroptosis in *FADD* KO embryos. (*A*) Representative pictures of mouse embryos with indicated *FADD* and *PUMA* genotypes at 13.5 d (E13.5). (*B*) Western blots of FADD and PUMA in E13.5 embryos with the indicated genotypes. (*C*) Expected and observed numbers of embryos with the indicated *FADD* and *PUMA* genotypes from 185 dissected E13.5 embryos. ***$P < 0.001$, $FADD^{-/-}/PUMA^{-/-}$ vs. $FADD^{-/-}/PUMA^{+/+}$; *NS*, $P = 0.5252$, $FADD^{-/-}/PUMA^{-/-}$ vs. the expected ratio of Mendelian inheritance (χ^2 test). (*D*) HMGB1 staining of fibroblast tissues from E13.5 embryos with the indicated genotypes. Arrowheads indicate cells with cytoplasmic HMGB1 staining and hollow nuclei. (Scale bars: 10 μm.) (*E*) Western blots of indicated proteins in E13.5 embryos with the indicated genotypes. (*F*) Model depicting the role of PUMA in necroptosis.

mitochondrial *CytB* and *NADH dehydrogenase 2* (*ND2*) genomic DNA, which requires the DNA-binding domain of DAI/Zbp1, was detected by immunoprecipitation in HT29 cells treated with L+Z (Fig. 5*E*). Knockdown of both *DAI/Zbp1* and *STING* abrogated necroptosis and RIP3/MLKL phosphorylation in HT29 cells, which was less affected by knockdown of either gene (Fig. 5*F*). Furthermore, *IFN-α* and *-β* were induced in necroptotic HT29 cells, which was suppressed by depletion of RIP3, PUMA, DAI/Zbp1, or STING (Fig. S7 *F* and *G*). Knockdown of *IFN-α/β receptor 1* (*IFNAR1*) reduced necroptosis in HT29 cells (Fig. S7 *H* and *I*). These results suggest that on activation by RIP3/MLKL, PUMA promotes mitochondrial DNA release and activation of DNA sensors, which cooperate to promote IFN response and enhanced RIP3/MLKL phosphorylation in a positive feedback loop.

***PUMA* KO Delays the Embryonic Lethality Caused by *FADD* KO.** The physiological role of RIP1/RIP3-mediated necroptosis has been demonstrated by mouse genetic studies in which RIP1 or RIP3 deficiency rescues developmental defects and/or embryonic death caused by deficiency in caspase 8 or FADD (29–31). To investigate the role of PUMA in necroptosis in vivo, we determined whether *PUMA* KO can also rescue the developmental defects in *FADD* KO mice (31). Genotyping of 102 newborn mice from the breeding of *PUMA* heterozygous ($PUMA^{+/-}$) and *FADD* heterozygous ($FADD^{+/-}$) mice did not identify any with the $FADD^{-/-}$ genotype, indicating that *PUMA* KO cannot rescue the postnatal lethality of *FADD* KO mice (31). Thus, we performed embryo dissection at several time points after pregnancy. Among 185 embryos dissected at E13.5, we identified 11 with the $FADD^{-/-}/PUMA^{-/-}$ DKO genotype (Fig. 6 *A* and *B* and Fig. S8*A*). This frequency (11 of 185) matched that of the Mendelian inheritance of *PUMA* KO and *FADD* KO alleles (Fig. 6*C*) and was statistically significant ($P < 0.001$, DKO vs. *FADD* KO). In contrast, only one (of 12 expected) $FADD^{-/-}/PUMA^{+/+}$ embryo and five $FADD^{-/-}/PUMA^{+/-}$ embryos (of 23 expected) were found (Fig. 6 *A*–*C* and Fig. S8*A*), suggesting a gene dosage effect of the *PUMA* KO allele. Despite being slightly smaller, the DKO embryos at embryonic day (E) 13.5 appeared to be grossly normal compared with WT embryos (Fig. 6*A*). Dissection at E11.5 recovered abnormally developed *FADD* KO embryos among completely normal-looking DKO embryos (Fig. S8*B*). H&E staining of embryonic tissues revealed massive cell loss in $FADD^{-/-}/PUMA^{+/-}$ embryos at E13.5, which was absent in the DKO embryos (Fig. S8*C*). In contrast to WT and DKO embryos with nuclear HMGB1, *FADD* KO embryos exhibited cytoplasmic HMGB1, suggestive of its release and necrotic death (Fig. 6*D*), which was also indicated by positive TUNEL staining but negative active caspase 3 staining (Fig. S8 *D* and *E*). Furthermore, DKO embryos exhibited reduced MLKL phosphorylation, DAI/Zbp1 induction, and STING depletion compared with *FADD* KO embryos (Fig. 6*E*). We also analyzed primary MEFs isolated from the embryos, and found that necroptosis induced by H_2O_2 or T+L+Z was substantially reduced in the DKO MEFs compared with *FADD* KO cells (Fig. S9). These results demonstrate that PUMA contributes to necroptosis in vivo and in vitro caused by *FADD* deficiency.

Discussion

Necroptosis and apoptosis share upstream pathways mediated by cell surface death receptors and can be triggered by a variety of stimuli that would normally induce apoptosis. On activation by TNF-α, RIP1 binds to and activates RIP3, which in turn activates MLKL by phosphorylation, leading to formation of a necrosome complex. RIP1 not only functions as a kinase to promote necroptosis, but also can act as a scaffold protein to inhibit necroptosis (24). The execution of necroptosis involves translocation of MLKL to the plasma and cytoplasmic membranes, where it promotes cell death through unclear mechanisms (32). Our results demonstrate that RIP3/MLKL-dependent PUMA induction promotes signal amplification in TNF-driven necroptosis in diverse cell types, such as epithelium, fibroblast, and developmental embryos. Unlike *RIP1* or *RIP3* KO, which rescues postnatal death of *FADD* KO mice (31), *PUMA* KO in mice partially rescues embryonic development before birth and after E13.5, consistent with its functional role in a rather late stage of necroptosis.

In addition to PUMA, several other Bcl-2 family members have been implicated in necroptosis. Bmf, also a BH3-only protein, was identified by a siRNA screen as being involved in TNF-α–induced necroptosis (12). Prosurvival proteins, such as Bcl-X_L, inhibit TNF-induced necroptosis (13). Unlike apoptosis, in which PUMA and other BH3-only proteins function through Bax/Bak to kill cells, necroptosis clearly does not require Bax and Bak (33), and can engage PUMA to kill *BAX/BAK*-deficient MEF and cancer cells (Fig. S6 *D* and *E*).

The induction of PUMA in necroptosis is mediated by MLKL through enhanced NF-κB activity and autocrine TNF-α signaling (Fig. 2). On RIP1/RIP3-mediated activation, MLKL oligomerizes and translocates to plasma and cytoplasmic membranes, where it promotes membrane rupture and release of cellular contents, including damage-associated molecular patterns (DAMPs) (34). These and other MLKL-mediated changes in early necroptosis can trigger inflammatory responses, which stimulate autocrine TNF-α and PUMA induction, leading to signal amplification in a positive feedback loop and eventual cell death (Fig. 6*F*). Autocrine TNF-α can be induced in response to IAP antagonists or excessive DNA damage (35), as well as in L929 cells undergoing necroptosis (36).

NF-κB–mediated transcription was also found to be involved in necroptosis induced by RIP3 oligomerization (37). However, adding exogenous TNF-α can make necroptosis less dependent on NF-κB–mediated transcription (Fig. 3*D* and Fig. S2*E*), likely related to enhanced initial MLKL phosphorylation (38).

Necroptosis can be triggered by exogenous viral DNA or bacterial infection (26); however, whether necroptosis signaling involves release of endogenous self-DNA is not quite clear. Our results suggest that PUMA promotes changes in mitochondrial morphology and cytosolic release of mitochondrial DNA to activate the DNA sensors DAI/Zbp1 and STING. PUMA was previously shown to promote mitochondrial fission (39), which can lead to release of mitochondrial DNA (40). On release, mitochondrial DNA, which shares common ancestry and homology with bacterial DNA, can act as an endogenous DAMP to activate innate immunity (41). Activation of DAI/Zbp1 and STING collectively promotes enhanced RIP3/MLKL phosphorylation (Fig. 6*F*). It is likely that DAI/Zbp1 does so by directly recruiting RIP3 through its RHIM domains (26). STING can be activated by cytosolic mitochondrial DNA (42) and mediate the IFN response in RIP3-dependent necroptosis on viral infection (27). Our data suggest that PUMA induces the STING-mediated IFN response to enhance RIP3/MLKL phosphorylation; however, the role of mitochondria in necroptosis is controversial and remains to be verified (43). Collectively, our results demonstrate that RIP3/MLKL-dependent PUMA induction promotes signal amplification and contributes to the execution of TNF-driven necroptosis in vitro and in vivo.

Materials and Methods

Cell Culture and Drug Treatment. Cells were maintained in a 37 °C incubator at 5% CO_2. Cell culture media were supplemented with 10% defined FBS (HyClone), 100 U/mL penicillin, and 100 μg/mL streptomycin (Invitrogen). Cells were plated and treated by drugs at 40–50% density in 12-well plates.

Analysis of Cell Viability and Death. Cell viability was analyzed by measuring ATP levels and crystal violet staining. Apoptosis was measured by counting cells with condensed and fragmented nuclei. Additional details are provided in *SI Materials and Methods*.

Analysis of Protein and mRNA Expression. Western blot analysis and real-time RT-PCR were performed as described previously (15).

Transfection and siRNA/shRNA Knockdown. Transfection of plasmids and siRNA was performed using Lipofectamine 2000 (Invitrogen) in accordance with the manufacturer's instructions.

Analysis of Mitochondrial DNA, Proteins, and Membrane Potential. Mitochondrial and cytosolic fractions were isolated by differential centrifugation as described previously (15). Additional details on mitochondrial analysis are provided in *SI Materials and Methods*.

Analysis of Mouse Embryos. All animal experiments were approved by the University of Pittsburgh's Institutional Animal Care and Use Committee. Additional details are in provided in *SI Materials and Methods*.

Statistical Analysis. Statistical analyses were performed using GraphPad Prism 4.

ACKNOWLEDGMENTS. We thank Xiaojun Chen, Ming Sun, and Kathy H. Y. Shair for providing technical assistance and Drs. Andrew Oberst and Douglas R. Green for sharing reagents. This work was supported by the National Institutes of Health (Grants CA172136, CA203028, and CA217141, to L.Z.; and U19AI068021, U01DK085570, and R01CA215481, to J.Y.). This work was performed using the UPMC Hillman Cancer Center shared facilities, supported in part by Award P30CA047904.

1. Ofengeim D, Yuan J (2013) Regulation of RIP1 kinase signalling at the crossroads of inflammation and cell death. *Nat Rev Mol Cell Biol* 14:727–736.
2. Pasparakis M, Vandenabeele P (2015) Necroptosis and its role in inflammation. *Nature* 517:311–320.
3. Linkermann A, Green DR (2014) Necroptosis. *N Engl J Med* 370:455–465.
4. Sun L, Wang X (2014) A new kind of cell suicide: Mechanisms and functions of programmed necrosis. *Trends Biochem Sci* 39:587–593.
5. He S, et al. (2009) Receptor interacting protein kinase-3 determines cellular necrotic response to TNF-alpha. *Cell* 137:1100–1111.
6. Zhang DW, et al. (2009) RIP3, an energy metabolism regulator that switches TNF-induced cell death from apoptosis to necrosis. *Science* 325:332–336.
7. Li J, et al. (2012) The RIP1/RIP3 necrosome forms a functional amyloid signaling complex required for programmed necrosis. *Cell* 150:339–350.
8. Sun L, et al. (2012) Mixed lineage kinase domain-like protein mediates necrosis signaling downstream of RIP3 kinase. *Cell* 148:213–227.
9. Wallach D, Kang TB, Dillon CP, Green DR (2016) Programmed necrosis in inflammation: Toward identification of the effector molecules. *Science* 352:aaf2154.
10. Czabotar PE, Lessene G, Strasser A, Adams JM (2014) Control of apoptosis by the BCL-2 protein family: Implications for physiology and therapy. *Nat Rev Mol Cell Biol* 15:49–63.
11. Yu J, Zhang L (2008) PUMA, a potent killer with or without p53. *Oncogene* 27(Suppl 1):S71–S83.
12. Hitomi J, et al. (2008) Identification of a molecular signaling network that regulates a cellular necrotic cell death pathway. *Cell* 135:1311–1323.
13. Irrinki KM, et al. (2011) Requirement of FADD, NEMO, and BAX/BAK for aberrant mitochondrial function in tumor necrosis factor alpha-induced necrosis. *Mol Cell Biol* 31:3745–3758.
14. Qiu W, et al. (2011) PUMA-mediated intestinal epithelial apoptosis contributes to ulcerative colitis in humans and mice. *J Clin Invest* 121:1722–1732.
15. Wang P, et al. (2009) PUMA is directly activated by NF-kappaB and contributes to TNF-alpha-induced apoptosis. *Cell Death Differ* 16:1192–1202.
16. Scaffidi P, Misteli T, Bianchi ME (2002) Release of chromatin protein HMGB1 by necrotic cells triggers inflammation. *Nature* 418:191–195.
17. Degterev A, et al. (2005) Chemical inhibitor of nonapoptotic cell death with therapeutic potential for ischemic brain injury. *Nat Chem Biol* 1:112–119.
18. Wu J, et al. (2013) Mlkl knockout mice demonstrate the indispensable role of Mlkl in necroptosis. *Cell Res* 23:994–1006.
19. Koo GB, et al. (2015) Methylation-dependent loss of RIP3 expression in cancer represses programmed necrosis in response to chemotherapeutics. *Cell Res* 25:707–725.
20. Bertrand MJ, et al. (2008) cIAP1 and cIAP2 facilitate cancer cell survival by functioning as E3 ligases that promote RIP1 ubiquitination. *Mol Cell* 30:689–700.
21. Dunai ZA, et al. (2012) Staurosporine induces necroptotic cell death under caspase-compromised conditions in U937 cells. *PLoS One* 7:e41945.
22. Dudgeon C, et al. (2010) PUMA induction by FoxO3a mediates the anticancer activities of the broad-range kinase inhibitor UCN-01. *Mol Cancer Ther* 9:2893–2902.
23. Tait SW, et al. (2013) Widespread mitochondrial depletion via mitophagy does not compromise necroptosis. *Cell Rep* 5:878–885.
24. Newton K, et al. (2016) RIPK1 inhibits ZBP1-driven necroptosis during development. *Nature* 540:129–133.
25. Wu J, Chen ZJ (2014) Innate immune sensing and signaling of cytosolic nucleic acids. *Annu Rev Immunol* 32:461–488.
26. Upton JW, Kaiser WJ, Mocarski ES (2012) DAI/ZBP1/DLM-1 complexes with RIP3 to mediate virus-induced programmed necrosis that is targeted by murine cytomegalovirus vIRA. *Cell Host Microbe* 11:290–297.
27. Schock SN, et al. (2017) Induction of necroptotic cell death by viral activation of the RIG-I or STING pathway. *Cell Death Differ* 24:615–625.
28. Konno H, Konno K, Barber GN (2013) Cyclic dinucleotides trigger ULK1 (ATG1) phosphorylation of STING to prevent sustained innate immune signaling. *Cell* 155:688–698.
29. Kaiser WJ, et al. (2011) RIP3 mediates the embryonic lethality of caspase-8-deficient mice. *Nature* 471:368–372.
30. Oberst A, et al. (2011) Catalytic activity of the caspase-8-FLIP(L) complex inhibits RIPK3-dependent necrosis. *Nature* 471:363–367.
31. Zhang H, et al. (2011) Functional complementation between FADD and RIP1 in embryos and lymphocytes. *Nature* 471:373–376.
32. Cai Z, et al. (2014) Plasma membrane translocation of trimerized MLKL protein is required for TNF-induced necroptosis. *Nat Cell Biol* 16:55–65.
33. Linkermann A, et al. (2013) Two independent pathways of regulated necrosis mediate ischemia-reperfusion injury. *Proc Natl Acad Sci USA* 110:12024–12029.
34. Zhang Y, Chen X, Gueydan C, Han J (2018) Plasma membrane changes during programmed cell deaths. *Cell Res* 28:9–21.
35. Biton S, Ashkenazi A (2011) NEMO and RIP1 control cell fate in response to extensive DNA damage via TNF-α feedforward signaling. *Cell* 145:92–103.
36. Christofferson DE, et al. (2012) A novel role for RIP1 kinase in mediating TNFα production. *Cell Death Dis* 3:e320.
37. Yatim N, et al. (2015) RIPK1 and NF-κB signaling in dying cells determines cross-priming of $CD8^+$ T cells. *Science* 350:328–334.
38. Wang H, et al. (2014) Mixed lineage kinase domain-like protein MLKL causes necrotic membrane disruption upon phosphorylation by RIP3. *Mol Cell* 54:133–146.
39. Din S, et al. (2013) Pim-1 preserves mitochondrial morphology by inhibiting dynamin-related protein 1 translocation. *Proc Natl Acad Sci USA* 110:5969–5974.
40. Mozdy AD, Shaw JM (2003) A fuzzy mitochondrial fusion apparatus comes into focus. *Nat Rev Mol Cell Biol* 4:468–478.
41. Zhang Q, et al. (2010) Circulating mitochondrial DAMPs cause inflammatory responses to injury. *Nature* 464:104–107.
42. Rongvaux A, et al. (2014) Apoptotic caspases prevent the induction of type I interferons by mitochondrial DNA. *Cell* 159:1563–1577.
43. Marshall KD, Baines CP (2014) Necroptosis: Is there a role for mitochondria? *Front Physiol* 5:323.